Agricultural and Forest Meteorology 274 (2019) 106–117

Contents lists available at ScienceDirect

Agricultural and Forest Meteorology

journal homepage: www.elsevier.com/locate/agrformet

Enhanced understory carbon flux components and robustness of net CO_2 exchange after thinning in a larch forest in central Japan

Munemasa Teramoto*, Naishen Liang*, Yoshiyuki Takahashi, Jiye Zeng, Nobuko Saigusa, Reiko Ide, Xin Zhao

Center for Global Environmental Research, National Institute for Environmental Studies, Tsukuba, Ibaraki, 305-8506, Japan

ARTICLE INFO

Keywords:
Automated chamber
Understory flux components
Soil respiration
Understory microclimate
Disturbance
Forest management

ABSTRACT

Thinning is a necessary procedure for the sustainable management of plantation forests. Thinning has a remarkable influence on forest carbon balance; however, there are limited studies showing the integrated assessment of the effects of thinning on several understory carbon flux components using long-term monitoring data. We measured understory flux components using automated chambers continuously over 12 years to understand the effects of forest thinning conducted in May 2014 and March 2015 and to elucidate the effect of short-term climate change on understory carbon balance in a Japanese larch (*Larix kaempferi* Sarg.) forest in central Japan. Although thinning (39% decrease in tree stems) increased the mean annual soil moisture by 16.5% and growing season soil temperature by 2.4%, large inter-annual variations in precipitation and soil temperature largely masked the effects of thinning on both soil respiration (R_s) and soil heterotrophic respiration (R_h). Annual mean soil temperature was positively related to all annual efflux components. Thinning also increased the understory photosynthetic photon flux density ($PPFD_u$) by 63.1% during the growing season (May to October). In post-thinning years, the average three-year understory photosynthesis (GPP_u), understory plant respiration (R_p), and total understory respiration (R_u) increased significantly by 59.5%, 99.7%, and 26.9%, respectively. The net understory CO_2 exchange (NUE = R_u − GPP_u) changed significantly only in 2015 (13.8%). A marginally significant change in NUE based on the three-year average in post-thinning years was also detected (14.4%). Our results indicated each flux component (especially GPP_u, R_p, and R_u) changed dramatically after thinning. In contrast, the NUE of this forest was relatively more robust than other enhanced understory flux components. However, the marginally significant increase of NUE (3-year average in post-thinning years) implied a slight increase in NUE after thinning.

1. Introduction

Forests cover about 30% of the land surface (FAO, 2015), and function as a carbon sink of 2.4 ± 0.4 Gt C per year (Pan et al., 2011). As emphasized in the Paris agreement, preservation and enhancement of the carbon sink capacity of forests is necessary for future adaptation and mitigation against global warming (Grassi et al., 2017). Plantations account for about 7% of global forests (FAO, 2015). Periodic forest thinning is necessary for sustainable management of plantations, because forests generally increase their carbon sequestration capacity after thinning (Ruiz-Peinado et al., 2017), as the growth rate of remaining trees is accelerated by improved partitioning of resources like radiation, soil nutrients, and water (Binkley et al., 2004), and more carbon is expected to be fixed by the remaining trees after thinning. This assumption of thinning effect on the forest carbon budget is mainly based on studies using tree census as a methodology (Morris et al., 1994; Peltola et al., 2002), or eddy-covariance flux monitoring (Dore et al., 2012; Saunders et al., 2012; Wilkinson et al., 2016). However, these measurement techniques cannot detect detailed changes in individual flux components after thinning. Understanding the detailed mechanism and response of each carbon flux component to thinning is necessary for developing effective and sustainable forest management strategies as mitigation and adaptation practices for a changing climate.

Understory carbon flux or net understory CO_2 exchange (NUE) comprises several flux components, including soil respiration (R_s), which is divided into soil heterotrophic respiration (R_h) and root respiration (R_r), understory gross primary production (GPP_u) and respiration of understory vegetation (R_p) (Teramoto et al., 2017). Some previous studies indicated that total understory respiration (R_u) accounts for more than half the ecosystem respiration in temperate forests

* Corresponding authors at: 16-2 Onogawa, Tsukuba, Ibaraki, 305-8506, Japan.
E-mail addresses: teramoto.munemasa@nies.go.jp (M. Teramoto), liang@nies.go.jp (N. Liang).

https://doi.org/10.1016/j.agrformet.2019.04.008
Received 11 December 2018; Received in revised form 5 April 2019; Accepted 8 April 2019
0168-1923/ © 2019 Elsevier B.V. All rights reserved.

Table 1
Canopy parameters and annual mean of environmental parameters in pre-thinning years (means ± SD for 8 years), in each year from 2013 to 2017, and in post-thinning years (means ± SD for 3 years). Values for solar radiation and $PPFD_u$ are the growing season average (May to October).

Year	Stems (ha^{-1})	DBH (cm)	Basal area ($m^2 ha^{-1}$)	Canopy height (m)	Tree LAI ($m^2 m^{-2}$)	Larch leaf litter ($t ha^{-1}$)	Above canopy air temp (°C)	Understory air temp (°C)	Soil temp (°C)	Soil moist (%)	Precipitation (mm)	Solar rad ($MJ m^{-2} d^{-1}$)	$PPFD_u$ ($\mu mol m^{-2} s^{-1}$)
Pre-thinning (2006-2013)					2.88	2.03 ± 0.31	9.46 ± 0.30	8.56 ± 0.33	8.94 ± 0.23	17.19 ± 0.97	1848 ± 275	15.12 ± 0.82	54.22 ± 7.25
2013	409	34.0	37.3	23.5		1.87	9.86	8.90	9.05	17.60	1839	16.17	60.56
2014	261	36.7	26.5			1.30	9.36	8.30	8.51	18.41	1788	16.02	73.30
2015	249	37.4	26.2		2.31	1.72	10.00	9.13	9.57	18.99	2031	15.75	88.12
2016	249	38.0	27.1	24.8		2.05	10.26	9.33	10.04	20.42	1484	15.19	90.52
2017							9.40	8.29	8.99	20.73	1735	15.34	85.03
Post-thinning (2015-2017)	249	37.7	26.7	24.8	2.31		9.89 ± 0.44	8.91 ± 0.55	9.53 ± 0.53	20.05 ± 0.93	1750 ± 274	15.42 ± 0.29	87.89 ± 2.75

(Yuste et al., 2005; Liang et al., 2010; Teramoto et al., 2016), and that GPP_u accounts for about 11–18% of ecosystem level gross primary production (GPP) in boreal forests (Swanson and Flanagan, 2001; Bergeron et al., 2009; Gaumont-Guay et al., 2009) and cool temperate forests (Teramoto et al., 2017). Therefore, the response of understory flux components to thinning strongly affects the forest carbon cycle after thinning. Thus, understory flux components are key elements for examining sustainable forest management under global climate change.

Thinning changes forest understory environmental parameters such as photosynthetic photon flux density ($PPFD_u$, Son et al., 2004), soil temperature (Lei et al., 2018), and soil moisture (Sundqvist et al., 2014). These changes are expected to influence understory carbon flux components. A meta-analysis by Zhang et al. (2018) showed that R_s generally increases in the early stage (less than two years) after thinning, and suggested that increased soil temperature, enhanced soil substrate availability, and dead root decomposition contributed to the increase in R_s. Additionally, an increase in understory photosynthesis induced by improved light conditions after thinning has also been suggested (Kolari et al., 2006; Teramoto et al., 2017). Several studies also reported that biomass (Son et al., 2004; Zhou et al., 2016) and photosynthetic carbon fixation capacity of understory vegetation (Cheng et al., 2017) was increased in post-thinning years. However, most previous studies focus only on part of the understory carbon flux components like R_s and R_h, and an integrated assessment of the thinning effect on multiple understory carbon fluxes that covers both respiratory and photosynthetic components is lacking so far.

Larch is a representative vegetation in the Eurasian continent and is an important plantation species in the northeast Asian region. In Japan, larch plantations were first initiated in the 1950s–1960s and occupy about 10×10^6 ha, which equals about 40% of total Japanese forests today (Forest Agency, 2012). The main goal of this study is to produce an integrated assessment of the thinning effect on the forest carbon cycle by focusing on understory carbon flux components for sustainable forest management under global climate change. Second, this study aims to detect the influence of short-term climate change on understory flux components using long-term monitoring data. We continuously measured the understory flux components like R_s, R_h, and NUE using a 24-channel automated chamber system for a duration of 12 years. Based on this 12-year dataset, we evaluated the influence of thinning on relevant environmental (biotic and abiotic) factors and understory carbon flux components by comparing the pre- and post- thinning periods. Our long-term dataset further allows us to capture the factors responsible for inter-annual variabilities in each understory flux component. To our knowledge, this is the first report on an integrated assessment of the thinning effect on understory flux components based on long-term continuous monitoring data.

2. Materials and methods

2.1. Site description

Data collection for this study began in 2006. The study site is a 56-year-old larch (*Larix kaempferi* Sarg.) plantation (at the start of measurement in 2006) at the northern foot of Mt. Fuji (35° 26′ 36.7″ N, 138° 45′ 53.0″ E; 1100 m asl), in Yamanashi Prefecture, central Japan (Fuji Hokuroku Flux Observation Site, http://asiaflux.net/index.php?page_id = 54; see Teramoto et al., 2017 for details). Briefly, in 2006, the canopy height, mean tree diameter at breast height (DBH), and stand density were 21.9 m, 31.8 cm, and 428 stems ha^{-1}, respectively. The basal area totalled 34.8 $m^2 ha^{-1}$. The leaf area index (LAI) during the growing season from May to October averaged 2.88 $m^2 m^{-2}$. The sub-canopy was scattered with Fuji cherry (*Prunus incisa*). The understory vegetation was composed of ferns (*Dryopteris crassirhizoma*) and a herb community (*Oplismenus undulatifolius*, *Carex japonica*, *Akebia quinata*, *Schisandra chinensis*, *Antenoron filiforme*, and *Rubus illecebrosus* (Arase, 2012). In addition, understory deciduous bush species (*Ilex*

serrata, *Deutzia crenata*, *Euonymus alatus*, *Zanthoxylum piperitum*, and *Callicarpa japonica*) were also present in a scattered distribution. Between 2006–2017 (the measurement period), the mean annual understory air temperature was 8.6 ± 0.4 °C, and the mean annual precipitation was 1819 ± 252 mm (average ± 1SD). The soil at our study site was a coarse-grained volcanic ash soil.

In May 2014 (the early growing season), about 36% of larch trees were thinned over 4 ha. However, thinning in the growing season strongly disturbs the forest floor. Therefore, larch trees inside the chamber measurement plot (size 55 × 55 m) were not thinned in 2014 (larch trees around chamber measurement plot were thinned). Larch trees inside the chamber measurement plot were thinned using the same approach in March 2015, soon after snow melt. About 39% of larch trees were cut in total from 2014 to 2015. Therefore, we defined the period from 2006 to 2013 and from 2015 to 2017 as pre-thinning years and post-thinning years, respectively. In addition, we regarded 2014 as in the middle of thinning process. The harvested timber and above-ground residues were taken from the research site for commercial use. The climate and biomass information before and after thinning is listed in Table 1.

2.2. Chamber measurement

We installed a multi-channel automated chamber system in the larch forest in April 2006, and continuously measured the understory carbon flux components such as R_s, R_h, and NUE. We installed 24 chambers including 16 soil chambers (90 cm in length × 90 cm in width × 50 cm in height) and eight plant chambers (90 cm in length × 90 cm in width × 100 cm in height). Eight of the soil chambers were assigned as control chambers to measure R_s and the other eight soil chambers were trenched chambers to measure R_h. The trench treatment was administered by cutting the roots around the trenched chambers with a chainsaw to a depth of 40 cm and inserting PVC plates around each trenched chamber to prevent root penetration. Surroundings of chambers were covered with soil to prevent air leaks. Understory vegetation in both control and trenched chambers was clipped every 2 weeks during the growing season. Plant chambers to measure NUE included understory vegetation with a height less than 100 cm. Chambers were made of plastic-coated steel frames (30 mm × 30 mm), transparent PVC walls (2 mm and 3 mm thick), and a PVC lid (3 mm thick). The transmittivity of PPFD through these PVC materials was 87.7 ± 0.6%, 83.3 ± 1.7%, and 79.7 ± 0.9% for the 2 mm thick wall, 3 mm thick wall, and 3 mm thick lid, respectively, under scattering light on a cloudy day. The transmittivity of PPFD was 83.3 ± 6.0%, 76.4 ± 2.9%, and 68.3 ± 2.3% for the 2 mm thick wall, 3 mm thick wall, and 3 mm thick lid, respectively, under direct sunlight on a sunny day.

All chambers were connected to a waterproof control unit. The main components of the control unit were a datalogger (CR1000, Campbell Scientific Inc., Logan, UT, USA), a micro-infrared gas analyser (IRGA; LI-820, LI-COR, Lincoln, NE, USA), a two valve-manifold (CKD-LAC-V-4SB010, CKD Corp., Nagoya, Japan), and a custom-made 62-differential-channel sensor multiplexer. Air temperature inside the chambers (25 cm and 50 cm above soil surface for soil and plant chambers, respectively) and soil temperature (5 cm depth) in all chambers was measured using thermocouples (T type). Soil moisture was measured using six TDR sensors (CS616, Campbell Scientific Inc.) at a depth of 10 cm in 6 randomly selected chambers (two chambers each for the control, trenched, and plant chambers). $PPFD_u$ at a height of 1 m was measured using 6 PAR sensors (SQ225; Apogee Instruments Inc., Logan, UT, USA) set around six randomly selected plant chambers. Only one chamber was kept closed for measurement, and the other 23 chambers were kept open. The chamber roof was automatically opened after measurement, and another chamber roof was automatically closed for the next measurement. In this study, measurement period in a chamber was 5 min (two hours for 24 chambers), and CO_2 data were recorded on a datalogger at 10 s intervals. For the detail of the measurement in pre-thinning years, see Teramoto et al. (2017).

2.3. Ecosystem photosynthesis (GPP)

To evaluate the changes in the contribution rate of GPP_u to GPP in post-thinning years, we used the GPP data measured by the eddy-covariance method. The eddy-covariance measurements were conducted about 50 m upwind from our chamber plots; see Takahashi et al. (2015) for details. We also used environmental data measured by the flux tower (understory air temperature, soil temperature, soil moisture, above canopy radiation, and $PPFD_u$) to fill the gaps in environmental data measured using the chamber system.

2.4. Measurement of understory plant biomass and larch leaf litter

We collected all above ground tissues (including litterfall) of the understory plants after the end of the growing season in 2017 to determine biomass, following the approach of Arase (2012). For this purpose, seven 2 × 2 m plots were sampled. In the laboratory, the collected samples were divided into herbaceous and woody tissues. Samples were air dried at 40 °C for 96 h and oven dried at 80 °C for 24 h, after which the dry weight was measured. We then compared the understory plant biomass data with that published by Arase (2012), collected pre-thinning. Arase (2012) reported only the biomass of understory herbaceous plant species and no pre-thinning data were available for understory wood plant species biomass; we therefore only compared the understory herbaceous plant species biomass in pre-thinning and post-thinning years. Litterfall was collected monthly using 12 litter traps (0.5 m^2 × 12). Collected litter was brought to the laboratory, and dry weight was measured.

2.5. Data processing and analysis

We followed the same procedure as that described by Teramoto et al. (2016, 2018) for the CO_2 flux calculation, temperature-response analysis, Q_{10} calculation, and moisture-response analyses. Briefly, we calculated the CO_2 flux (F_c, μmol CO_2 m^{-2} s^{-1}) of each chamber using the following equation:

$$F_c = \frac{P_0 V}{RS(T_{air} + 273.15)} \frac{\partial C}{\partial t} \quad (1)$$

where P_0 is the air pressure (Pa), V is the effective chamber volume (m^3), R is the ideal gas constant (8.314 Pa m^3 K^{-1} mol^{-1}), S is the measured soil surface area (m^2), T_{air} is the air temperature (°C), and $\partial C/\partial t$ is the rate of change of the CO_2 molar fraction (μmol mol^{-1} s^{-1}). We identified the outliers of CO_2 data points during measurement in a chamber using linear regression of CO_2 against the closure time. If a difference (the difference between the estimated CO_2 concentration by linear regression and the measured CO_2 concentration) were larger than three times the standard deviation (3σ) of residuals during the measurement, we identified the data point as an outlier. We repeated the regression analysis and removal of outlier data points twice. After the removal of outliers, we calculated the goodness of fit (correlation coefficient, R) for the linear regression of CO_2 concentration as a function of time. If the R was below 0.95, we did not use the flux data for analysis because low values of R indicate mechanical trouble in the system. In the case of plant chambers, we applied the same data quality check procedure for night time data ($PPFD_u$ < 2.0). If we could not obtain good quality night time data (R > 0.95) in a day, we also did not use day time data from the chamber on that day. Additional details of data processing and analysis can be found in a recent publication by Liang et al. (2017).

To analyse the temperature response of F_c and to fill gaps in the respiration data, we used the following model (Lloyd and Taylor, 1994):

$$F_c = R_{ref} e^{E_0 \times \left(\frac{1}{T_{ref} - T_0} - \frac{1}{T_s - T_0}\right)} \quad (2)$$

where R_{ref} (μmol CO_2 m^{-2} s^{-1}) is the CO_2 efflux at a specified reference soil temperature (T_{ref}: 283.15 K), E_0 is a fitting parameter, T_0 is the soil temperature when F_c is zero (227.13 K), and T_s is the observed soil temperature (K). For the plant chambers, we used nocturnal data for the temperature and moisture response analysis. To analyse the temperature sensitivity of F_c in each chamber and treatment, we used regression analysis with the following exponential model:

$$F_c = R_{15} e^{b(T_s - 15)} \quad (3)$$

where R_{15} is the CO_2 efflux at 15 °C (μmol CO_2 m^{-2} s^{-1}), b is a fitting parameter for temperature sensitivity, and T_s is the soil temperature (°C) from Eq. (2). From Eq. (3), the change in soil CO_2 efflux per 10 °C change in soil temperature (Q_{10}) is calculated as follows:

$$Q_{10} = e^{10b} \quad (4)$$

We used this equation to derive annual Q_{10} values from the annual temperature response curve for F_c. We used Eq. (2) for filling gaps in F_c because fitting was slightly better in Eq. (2) than in Eq. (3).

To avoid the confounding effect of soil temperature and soil moisture, we first subtracted the simulated value of F_c (based on Eq. (2)) from the observed value. The residual values (the temperature-normalized F_c: RF_c, μmol CO_2 m^{-2} s^{-1}) were used to analyse the relationship between soil moisture and F_c. As Harper et al. (2005) indicated, soil CO_2 efflux is suppressed under dry or excessively moist conditions, and peaks under intermediate soil moisture conditions. Therefore, quadratic Eq. (5) fit well with the soil moisture response of RF_c.

$$RF_c = c_1 \theta^2 + c_2 \theta + c_3 (c_1 < 0) \quad (5)$$

where θ is the volumetric soil moisture (%) and c_1, c_2, and c_3 are fitting parameters. However, when $c_1 \geq 0$ in Eq. (5), the equation means that RF_c will increase under dry or excessively moist conditions, and mislead the soil moisture response of RF_c. Therefore, in that case ($c_1 \geq 0$ in Eq. (5)), we used the following linear regression instead:

$$RF_c = c_1 \theta + c_2 \quad (6)$$

In this study site, F_c values were rapidly increased after heavy rain (> 10 mm hr^{-1}). Such rapid and short increases of F_c (lasted for several minutes to hours) were considered to be caused by soil pore degassing due to rain water (physical displacement) and were different from the soil moisture response of respiratory flux components associated with biotic factors like activation of soil microbiota and living roots (usually lasts for several hours to days, Liu et al., 2002). Therefore, we separated the rapidly increased F_c after heavy rainfall (> 10 mm hr^{-1}) from other data when we conducted regression analysis of soil moisture response of F_c following the procedure of Teramoto et al. (2017).

Daytime F_c data from the plant chamber represent NUE, and nocturnal F_c represents understory respiration (R_u). Understory GPP (GPP_u, μmol CO_2 m^{-2} s^{-1}) was calculated using the following equation:

$$GPP_u = R_u - NUE \quad (7)$$

In this equation, daytime R_u was estimated from the temperature response of nocturnal F_c in plant chambers using Eq. (2). Estimating R_p only from plant chambers was difficult, so we used the following equation to quantitatively calculate R_p.

$$R_p = R_u - R_s \quad (8)$$

In Eq. (8), we regarded R_s in soil chambers and plant chambers were equal even though we admitted possible uncertainty due to the influence of litter input from understory plant species on R_h in plant chambers. One plant chamber was damaged by a falling tree, and we could not get good quality data from the chamber in post-thinning years. As a result, we used 8, 8, and 7 of control chambers, trenched chambers, and plant chambers, respectively, for the analysis in this study. Differences in environmental data and flux data (includes annually summed flux data, Q_{10} and R_{15} data) between pre-thinning years (from 2006 to 2013) and from 2014 to 2017 were statistically analysed using a two-tailed paired t-test ($p < 0.10$) after normality testing with Shapiro-Wilk tests ($p < 0.05$). If data set did not pass the normality test, Wilcoxon Signed Rank Test was conducted ($p < 0.10$). All the statistical and regression analyses were performed using version 10.0 of SigmaPlot software (Systat Software, San Jose, CA, USA).

2.6. Gap filling for the flux data

The gap filling method in this study (from 2014 to 2017) is same as that used in a previous report in pre-thinning years (Teramoto et al., 2017). Briefly, missing F_c data (gaps caused by snow fall or mechanical trouble) for R_s and R_h were estimated based on the annual temperature-response equation derived from Eq. (2) in each chamber. Gap filling of R_u (including daytime R_u) was performed using nocturnal data similar to the gap filling for R_s and R_h. To fill the GPP_u gaps, we applied the artificial neural network model of Zeng et al. (2014) for each plant chamber. Two-hourly soil temperature data from each chamber, soil moisture content, the mean $PPFD_u$ for the study site, and the GPP_u from each chamber were used to train the model using the annual data in 2014 (to simulate GPP_u in 2014) and all the data for three years from 2015 to 2017 (to simulate GPP_u in post-thinning years). In addition, we incorporated seasonal functions (m and n in the following Eqs. 9 and 10) in the training and simulation components of the model:

$$m = \cos\left(2\pi DOY / 365\right) \quad (9)$$

$$n = \sin\left(2\pi DOY / 365\right) \quad (10)$$

where DOY is the day of the year. Two-hourly m and n are used for training the model with other above-mentioned parameters. After training the model, two-hourly GPP_u in each chamber was simulated using two-hourly soil temperature data from each chamber, the soil moisture content, the mean $PPFD_u$ for the study site, and seasonal functions (m and n). We filled the NUE gaps using the gap-filled R_u and GPP_u values from Eq. (7). Data gaps existed mainly during the snow-covered period (because snow changes chamber volume and causes overestimation of F_c), particularly from January to February in each year, and a gap filling procedure was applied.

2.7. Evaluation of thinning effect on understory climatic factors and flux components

We examined the thinning effect on understory climatic factors and flux components by comparing the average values for 8 years in pre-thinning years and values in each year from 2014 to 2017. The study site was a matured larch forest (56-year-old in 2006), and inter-annual variation of understory flux components in pre-thinning years were largely controlled by climatic factors like mean annual soil temperature (R_s, R_h, NUE, and R_u) and average value of $PPFD_u$ during the growing season (GPP_u) (Teramoto et al., 2017). Therefore, the influence of inter-annual variation of climatic factors on the evaluation of thinning effect was high if we used one-year data in pre-thinning years for the comparison. Especially in 2013 (the year just before thinning started in 2014), there was a short drought in summer, and the average radiation during the growing season in 2013 was the highest among 8 years in pre-thinning years (Teramoto et al., 2017). To remove the influence of inter-annual variation from the evaluation of thinning effect on understory climatic factors and flux components as possible, we used average values for 8-years as a representative of the pre-thinning years. We compared environmental parameters and flux values between pre-thinning years and the years from 2014 to 2017 in each sensor and chamber, and calculated the change ratio (average of change ratio ± 1SD).

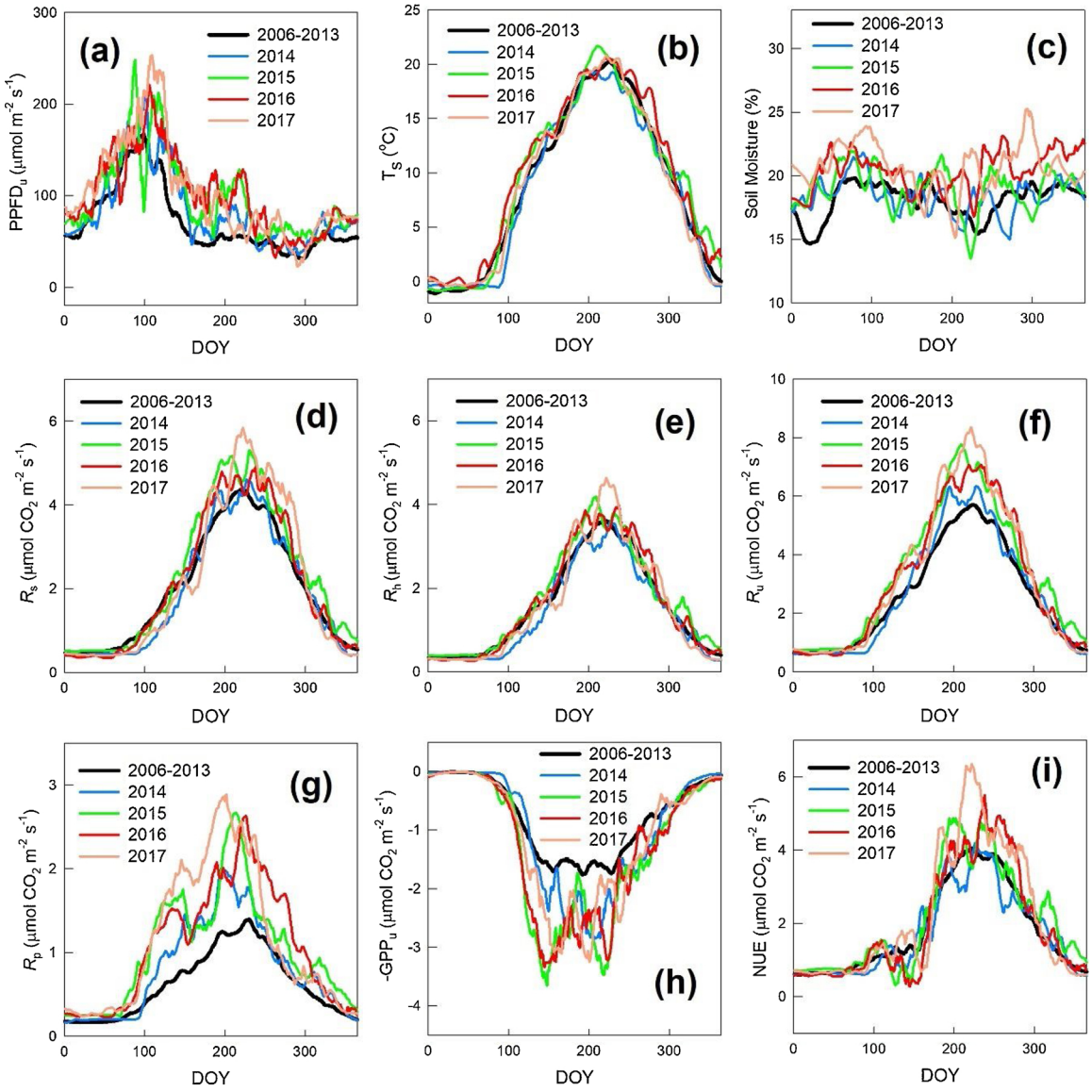

Fig. 1. Time series (11-day moving window) in the pre-thinning years (average for 8 years) and in each year from 2014 to 2017 for (a) $PPFD_u$, (b) soil temperature (Ts), (c) soil moisture, (d) soil respiration (R_s), (e) soil heterotrophic respiration (R_h), (f) understory respiration (R_u), (g) plant respiration (R_p), (h) understory gross primary production (GPP_u), and (i) net understory CO_2 exchange (NUE). .

Table 2
Averaged relative ratio of annual means of environmental parameters and understory flux components in the years 2014–2017 to the average of the pre-thinning years for 8 years (mean ± 1SD). The averages of parameters in the post-thinning years (2015–2017) were also compared with those of the pre-thinning years.

Year	N	2014	2015	2016	2017	Post-thinning (2015-2017)
Above canopy air temp	1	0.989	1.057	1.085	0.993	1.045
Understory air temp	23	0.962 ± 0.010***	1.069 ± 0.007***	1.084 ± 0.011***	0.988 ± 0.009***	1.047 ± 0.007***
Soil temp	23	0.951 ± 0.018***	1.071 ± 0.028***	1.124 ± 0.040***	1.007 ± 0.035	1.067 ± 0.033***
Soil moist	6	1.071 ± 0.055**	1.104 ± 0.063**	1.187 ± 0.061***	1.205 ± 0.059***	1.165 ± 0.055***
$PPFD_u$	5	1.354 ± 0.133***	1.639 ± 0.260***	1.679 ± 0.227***	1.576 ± 0.186***	1.631 ± 0.223***
R_s	8	0.971 ± 0.174	1.176 ± 0.203**	1.081 ± 0.183	1.093 ± 0.252	1.117 ± 0.175
R_h	8	0.876 ± 0.121**	1.080 ± 0.176	1.053 ± 0.153	1.002 ± 0.227	1.045 ± 0.176
R_u	7	1.042 ± 0.119	1.290 ± 0.112***	1.239 ± 0.142***	1.280 ± 0.235**	1.269 ± 0.137***
R_p	7	1.349 ± 0.509	1.840 ± 0.684***	1.887 ± 0.736**	2.264 ± 1.245*	1.997 ± 0.791***
GPP_u	7	1.262 ± 0.204**	1.669 ± 0.330***	1.648 ± 0.390***	1.468 ± 0.464**	1.595 ± 0.376***
NUE	7	0.947 ± 0.167	1.138 ± 0.130**	1.074 ± 0.146	1.220 ± 0.337	1.144 ± 0.176*

*, **, and *** represent significant differences of the indicated parameter compared with the pre-thinning years at $p < 0.10$, $p < 0.05$, and $p < 0.01$, respectively. Values for $PPFD_u$ are growing season averages (May to October). N indicates the number of replicates for each parameter.

3. Results

3.1. Changes in environmental conditions before and after thinning

Thinning decreased the stand density, basal area, and canopy LAI by about 39%, 30%, and 20%, respectively (based on the data in 2013 and 2015 in Table 1). Decrease in these canopy parameters did not change the seasonal patterns of understory environmental factors like understory PPFD ($PPFD_u$), soil temperature, and soil moisture. $PPFD_u$ peaked in early to middle April and decreased after the leafing of larch trees in late April (Fig. 1a). Soil temperature was around 0 °C during the snow-covered period from January to February, and gradually increased after snow melt in March to early April and peaked in August (Fig. 1b). The seasonal variation in soil moisture was not as clear as for $PPFD_u$ and soil temperature, but soil moisture generally showed a decreasing trend from July to August (Fig. 1c).

Thinning significantly increased the average value of $PPFD_u$ during the growing season by 35.4% (+ 19.08 μmol m^{-2} s^{-1}) in 2014 (Tables 1 and 2). The ratio of increase in $PPFD_u$ was further increased to 57.6–67.9% (+30.80 to + 36.30 μmol m^{-2} s^{-1}, + 33.67 μmol m^{-2} s^{-1} for 3-year average) from 2015 to 2017 (Tables 1 and 2). Mean annual soil temperature (MAT) decreased by 4.9% (−0.44 °C) in 2014, compared to that in pre-thinning years (Tables 1 and 2), but MAT was significantly increased (6.7%) in post-thinning years (2015–2017; +0.59 °C, Tables 1 and 2). Extracting the effect of thinning on MATs and excluding the influence of inter-annual variation in MATs were difficult because the amount of snowfall and the timing of snow melt was different in each year. Therefore, we estimated the effect of thinning on soil temperature during the growing season. We analysed the relationship between the daily average of above canopy air temperature and soil temperature during the growing season in pre-thinning years, and subtracted the estimated soil temperature from the observed soil temperature from 2014 to 2017. The average of residual values of soil temperature in post-thinning years was +0.37 °C (2.4% of soil temperature during growing season in pre-thinning years). The annual mean soil moisture increased significantly in post-thinning years from 10.4 to 20.5% (+1.80 to +3.54% as the annual mean of soil moisture value, Tables 1 and 2). However, annual precipitation in post-thinning years (1750 mm) was less than the annual precipitation in pre-thinning years (1848 mm). Average values for mean soil moisture during the growing season for 3 years in post-thinning years were 19.94 ± 0.27%, 20.77 ± 2.04%, and 17.83 ± 0.41% in control, trenched, and plant chambers, respectively.

3.2. Changes in understory flux components before and after thinning

Seasonal patterns of understory efflux components (R_s, R_h, R_u and R_p) largely corresponded to the seasonal patterns in soil temperature (Fig. 1d–g). The GPP_u of pre-thinning years was increased during April to May and peaked in July to August (Fig. 1h). In post-thinning years, the increase of GPP_u in May was further enhanced. GPP_u peaks in post-thinning years were seen in May (2015), June (2016), or July (2017) (Fig. 1h). The high level of GPP_u was maintained until August, and GPP_u decreased from September to December, similar to the seasonal pattern in pre-thinning years (Fig. 1h). NUE of the post-thinning years increased from April, similar to the pre-thinning years, but it was remarkably decreased in May (monthly NUE values were the smallest in May in 2015 and 2016) and remained low until June due to enhanced GPP_u. NUE of the post-thinning years remarkably increased from June to July and peaked in July (2015), August (2017), and September (2016). After those peaks, NUE of the post-thinning years decreased continuously until December, similar to the pre-thinning years (Fig. 1i).

The annual sums of understory CO_2 fluxes in the pre-thinning years and the years from 2014 to 2017 are shown in Fig. 2. Compared with the pre-thinning years, the annual R_s was significantly increased in 2015 (17.6%, Table 2). Annual R_h was significantly lower in 2014 (-12.4%, Table 2), but the change in annual R_h in post-thinning years was not significant. Annual R_u (23.9–29.0% in the post-thinning years and 26.9% for the three-year average from 2015 to 2017, Table 2), annual R_p (84.0–126.4% in post-thinning years and 99.7% for three-year average from 2015 to 2017, Table 2), and annual GPP_u (26.2% in 2014, 46.8–66.9% in post-thinning years and 59.5% for three-year average from 2015 to 2017, Table 2) were significantly higher after thinning. NUE was significantly higher in 2015 (13.8%, Table 2) compared to that in the pre-thinning years, and a marginally significant increase in NUE based on the three-year average in the post-thinning years (14.4%, Table 2) was detected.

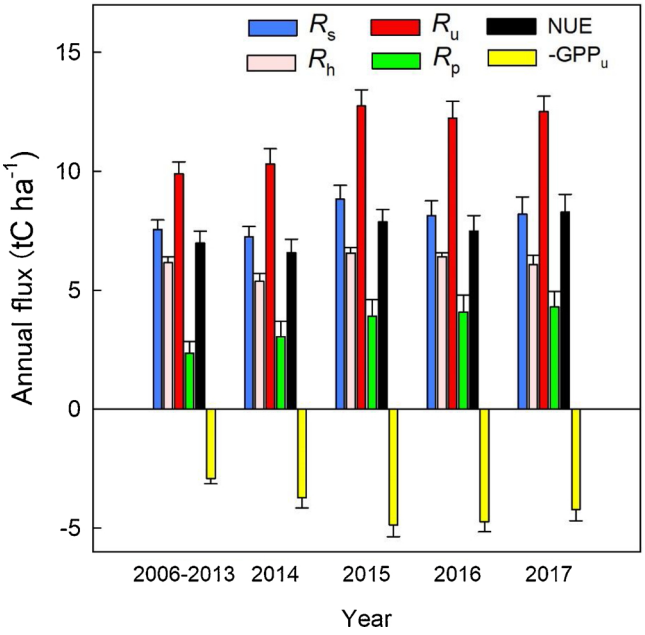

Fig. 2. Annul sum of understory flux components in pre-thinning years and from 2014 to 2017. Values are represented as mean ± SE.

3.3. Temperature response of understory efflux components

Understory CO_2 efflux components (R_s, R_h, and R_u) increased exponentially along with the seasonal soil temperature increase each year after thinning (Fig. 3). Thinning did not significantly affect R_{15} (estimated CO_2 efflux at 15 °C) of R_s and R_h from 2014 to 2017 (Table 3). On the other hand, R_{15} of R_u significantly increased from 2014 to 2017 (Table 3). Annual Q_{10} of R_s (increased from 2014 to 2017, except in 2015), R_h (marginally increased in 2016), R_u (increased from 2014 to 2017 except 2015) were higher from 2014 to 2017 compared with the values in the pre-thinning years.

Annual sums of efflux components increased exponentially along with the increase in MATs (Fig. 4a–d). Annual R_s and R_h in the post-thinning years were in the range of the 95% prediction interval based on the relationship between MATs and annual F_c values in the pre-thinning years, except in 2016 (Fig. 4a, b). Annual R_s and R_h in 2016 lay outside the 95% prediction interval, and the annual values were lower than the value estimated from the MATs-annual F_c relationship (Fig. 4a, b). Therefore, when data from 2014 to 2017 were included in the analysis, the exponential regression curves became less steep compared with those of the pre-thinning years (Fig. 4a, b). On the other hand, annual R_u values in 2015 and 2017 lay outside the 95% prediction interval, and were higher than the values estimated from the MATs-annual F_c relationship (Fig. 4c). Therefore, when data from 2014 to 2017 were included in the analysis, the exponential regression curve became steeper compared with that in the pre-thinning years (Fig. 4c). Annual R_p was not significantly related with MATs in the pre-thinning

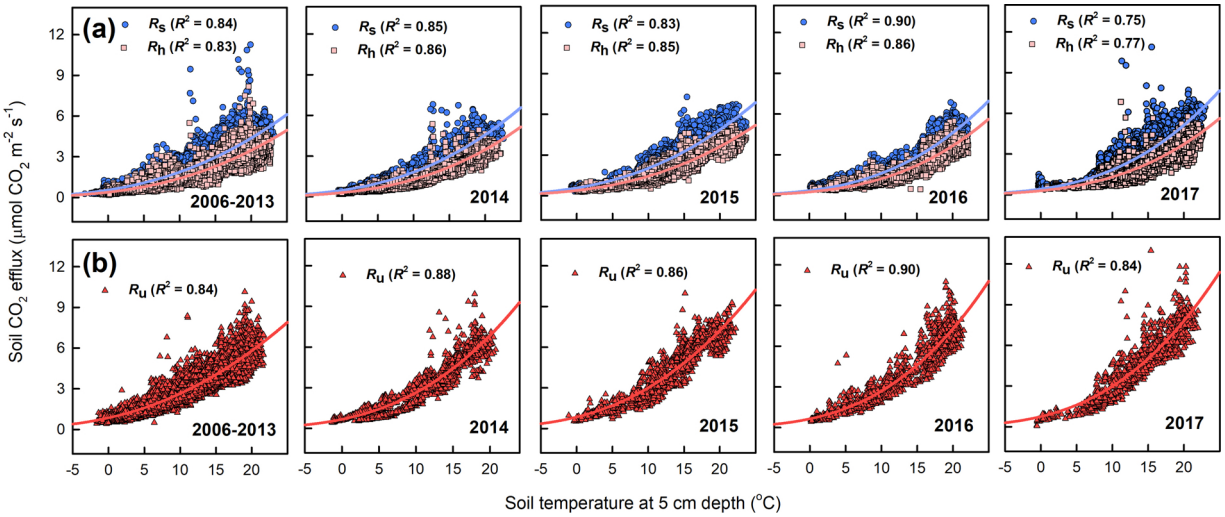

Fig. 3. Seasonal temperature response of (a) soil respiration (R_s) and soil heterotrophic respiration (R_h) and (b) understory respiration (R_u). For R_u, nocturnal data were plotted in the figure. In the pre-thinning years (2006–2013), all data for 8 years were plotted. All exponential regression curves (Eq. (2) was used for the fitting) were significant at $p < 0.001$. Each symbol represents the mean of chambers (n = 8 for R_s and R_h, n = 7 for R_u).

years. However, annual R_p was significantly related with MATs when the data from 2014 to 2017 were included in the regression analysis (Fig. 4d).

3.4. Soil moisture response of understory efflux components

R^2 values for relationships between soil moisture and understory CO_2 effluxes (R_s, R_h and R_u) from July to September 2014 to 2017, were less than 0.40 (Fig. 5). Except for R_p, there was no significant relationship between the annual understory CO_2 efflux components (R_s, R_h, and R_u) and average soil moisture from March to November when the data from 2014 to 2017 were included in the analysis (Fig. 6). Annual R_p was the only efflux component that was positively related to the average soil moisture from March to November even though there was no significant relationship in pre-thinning years (Fig. 6d).

3.5. Light response of understory photosynthesis and biomass

In 2017, understory herbaceous plant biomass was 281.0 ± 25.6 g m^{-2} (ranged from 220.1 to 364.3 g m^{-2}, mean ± SE) and woody plant biomass was 586.0 ± 346.6 g m^{-2} (ranged from 4.2 to 2292.8 g m^{-2}, mean ± SE). $PPFD_u$ was positively related with both summed GPP_u and R_p during the growing season (Fig. 7).

The contribution of GPP_u to GPP (GPP_u:GPP ratio) was significantly increased from 2014 to 2016 compared with that in pre-thinning years (Fig. 8). In pre-thinning years, the GPP_u:GPP ratio was 14.2 ± 1.2% (mean ± SE). The GPP_u:GPP ratio significantly increased to 24.5 ± 2.9% ($p = 0.002$), 23.8 ± 2.5% ($p = 0.002$), and 23.0 ± 2.0% ($p = 0.002$) in 2014, 2015, and 2016, respectively (mean ± SE). In 2017, the GPP_u:GPP ratio was marginally higher than that in the pre-thinning years (19.2 ± 2.2%, mean ± SE, $p = 0.058$).

4. Discussion

4.1. Impact of thinning on the temperature and moisture response of understory efflux components

Thinning increased the average growing season soil temperatures by 0.37 °C (2.4%) compared to the pre-thinning years, likely due to increased incident solar radiation after thinning. A recent study by Lei et al. (2018) reports similar results: 15% thinning increased MATs by 0.34 °C (2.4%) in a 43-year-old pine forest.

After thinning, soil moisture increased even though the annual precipitation was lower in post-thinning years (1750 mm) compared to pre-thinning years (1848 mm). Increased soil moisture after thinning is also reported in previous studies (Sundqvist et al., 2014; Lei et al., 2018). This can be explained by decreased transpiration in the forest as a result of thinning. In fact, Sun et al. (2017b) demonstrated that the ratio of transpiration in evapotranspiration decreased from 45.0 to 34.9% and the annual evapotranspiration also decreased by 20.4% due to 50% strip thinning in a Japanese cypress plantation.

Our results suggest that soil temperature is the primary factor that controls seasonal and annual understory efflux components, especially for R_s and R_h (Figs. 3 and 4). On the contrary, influence of soil moisture on seasonal changes of understory efflux components was relatively weak compared with soil temperature (Fig. 5). In addition, most of the

Table 3
Values of R_{15} and Q_{10} for understory efflux components. In pre-thinning years, all the data from 2006 to 2013 (average ± SE) were used for each component. From 2014 to 2017, annual data were used for each year.

	R_{15} (μmol CO_2 m^{-2} s^{-1})			Q_{10}		
Year	R_s	R_h	R_u	R_s	R_h	R_u
Pre-thinning (2006-2013)	2.85 ± 0.13	2.25 ± 0.09	3.94 ± 0.39	2.37 ± 0.08	2.51 ± 0.08	2.38 ± 0.08
2014	2.89 ± 0.17	2.12 ± 0.13	4.27 ± 0.28*	2.61 ± 0.10***	2.77 ± 0.09	2.70 ± 0.08***
2015	3.17 ± 0.20	2.33 ± 0.07	4.69 ± 0.25***	2.33 ± 0.05	2.38 ± 0.06	2.40 ± 0.06
2016	2.77 ± 0.20	2.17 ± 0.05	4.33 ± 0.24**	2.76 ± 0.10***	2.85 ± 0.13*	2.84 ± 0.12***
2017	3.12 ± 0.26	2.27 ± 0.16	4.88 ± 0.22**	2.70 ± 0.07***	2.64 ± 0.10	2.63 ± 0.08***
Post-thinning (2015-2017)	3.04 ± 0.19	2.29 ± 0.08	4.66 ± 0.19***	2.53 ± 0.06**	2.59 ± 0.08	2.59 ± 0.07***

*, **, and *** represent a significant difference of the indicated parameter compared with the pre-thinning years, at $p < 0.10$, $p < 0.05$, and $p < 0.01$, respectively.

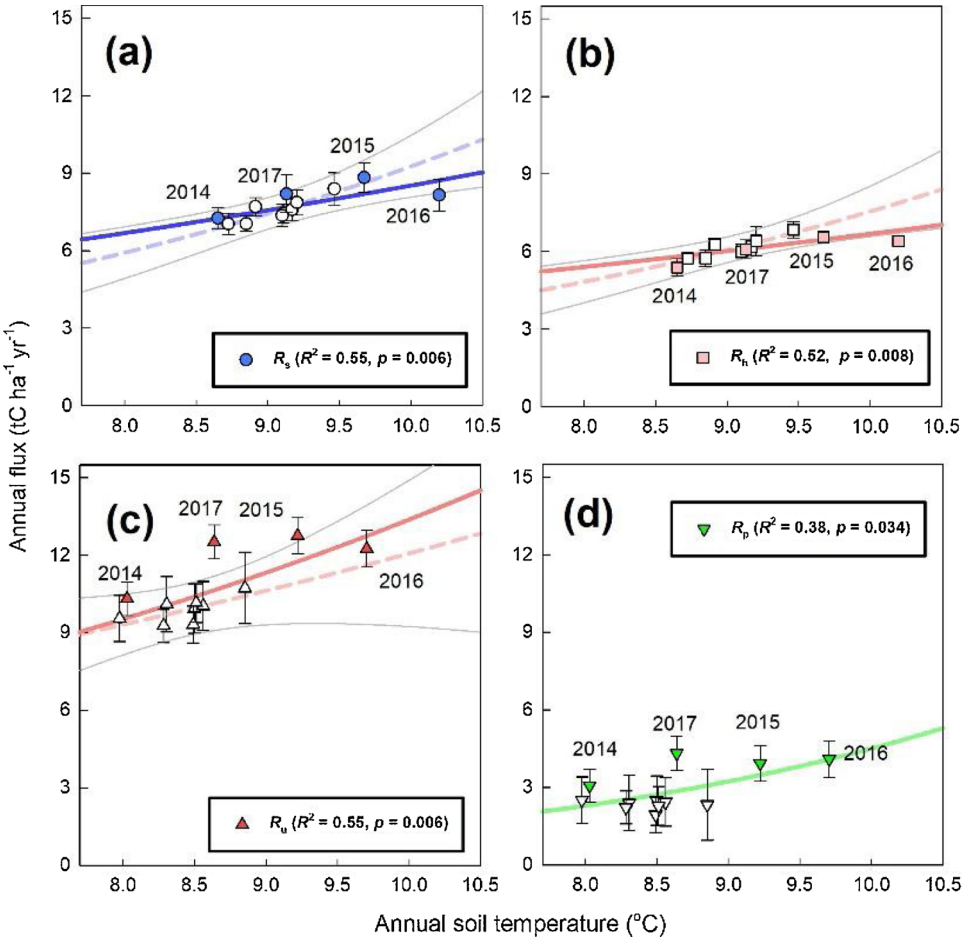

Fig. 4. Relationships between mean annual soil temperature (MATs) and annual sum of understory efflux components: (a) soil respiration (R_s), (b) soil heterotrophic respiration (R_h), (c) understory respiration (R_u) and (d) plant respiration (R_p). Empty symbols represent data in the pre-thinning years and filled symbols represent data from 2014 to 2017. Dashed curves represent significant ($p < 0.10$) relationships between MATs and each efflux component in the pre-thinning years as shown in Teramoto et al. (2017), and coloured solid curves represent significant relationships between MATs and each efflux component, including all the data for 12 years of measurement. Pairs of grey curves show the 95% prediction intervals based on regression analysis in the pre-thinning years. Values are represented as mean ± SE.

annual efflux components did not respond to soil moisture increase in the post-thinning years (Fig. 6a–c). This is because the inter-annual negative relationships between soil moisture and efflux components in pre-thinning years were mainly caused by inter-annual variation in soil temperature (average values of soil temperature and soil moisture from March to November were negatively related in pre-thinning years), as indicated by Teramoto et al. (2017). However, in post-thinning years, there was no significant relationship between soil temperature and soil moisture because soil moisture increased in the post-thinning years due to decreased transpiration.

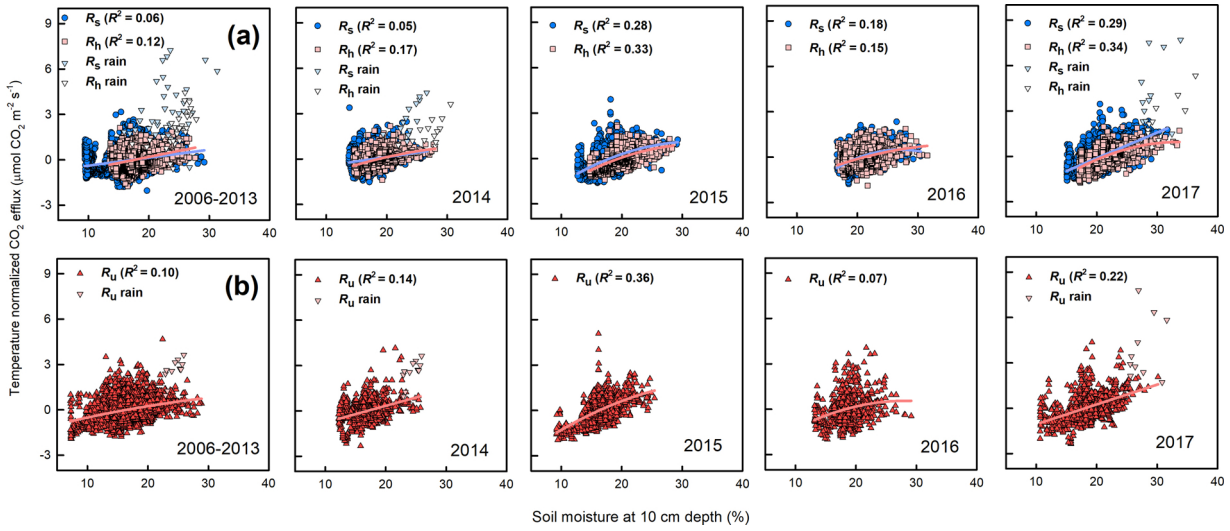

Fig. 5. Soil moisture response of temperature normalized CO_2 efflux (RF_c in Eqs. (5) and (6)) of (a) soil respiration (R_s) and soil heterotrophic respiration (R_h) and (b) understory respiration (R_u) during the growing season from May to October. For R_u, only the nocturnal data (night time NUE) was plotted in the figure. Rapid and short increases of understory effluxes that occurred immediately after heavy rainfall (> 10 mm h^{-1}, "R_s rain," "R_h rain," and "R_u rain"; inverted triangles) were not included in the regression analysis. In the pre-thinning years (2006–2013), all the data for 8 years were plotted. All regression curves and lines were significant at $p < 0.001$. Each symbol represents the mean of chambers (n = 8 for R_s and R_h, n = 7 for R_u).

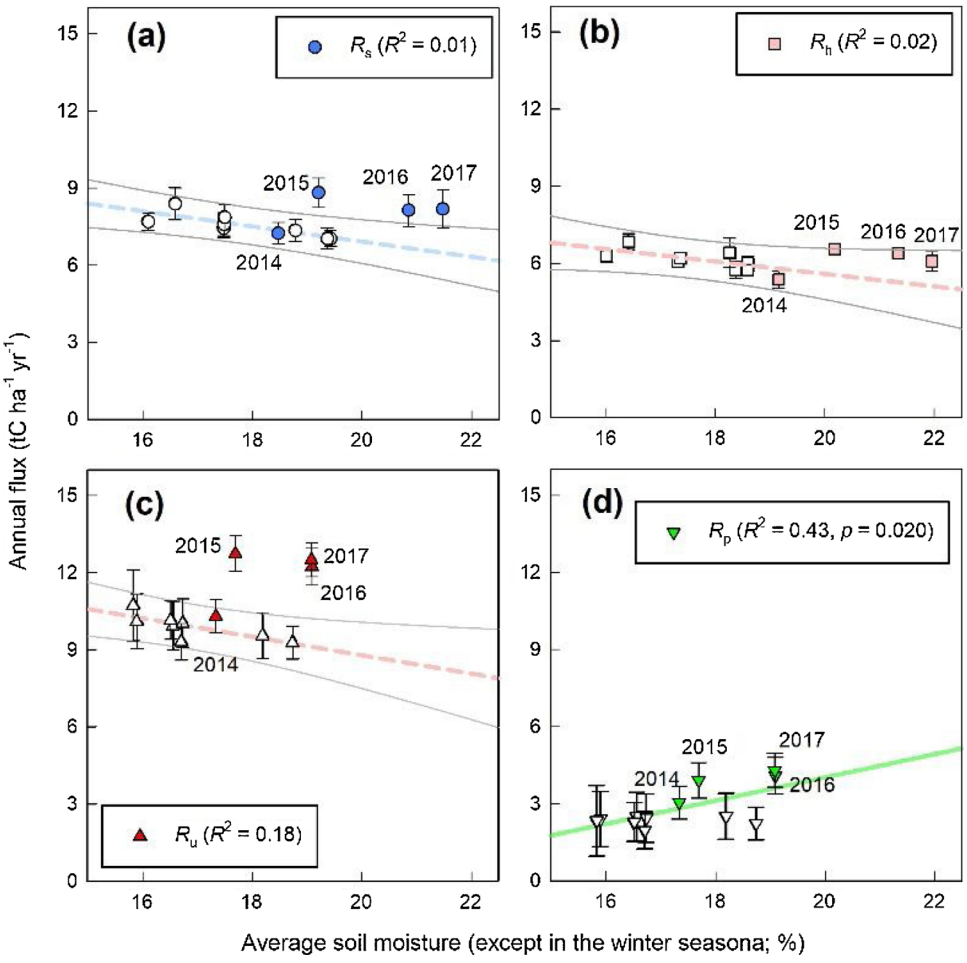

Fig. 6. Relationships between the annual mean soil moisture (except the soil frozen and snow-covered period from December to February) and annual (a) soil respiration (R_s), (b) soil heterotrophic respiration (R_h), (c) understory respiration (R_u), and (d) plant respiration (R_p). Empty symbols represent data of the pre-thinning years and filled symbols represent data from 2014 to 2017. Dashed lines represent significant ($p < 0.10$) relationships between soil moisture and each efflux component in pre-thinning years as shown in Teramoto et al. (2017), and coloured solid line represent significant relationships between soil moisture and each efflux component including all the data for 12 years of measurement. Pairs of grey curves show 95% prediction intervals based on regression analysis in pre-thinning years. Values are mean ± SE.

Annual Q_{10} in R_s, R_h, and R_u showed significant or marginally significant increase in post-thinning years. Previous studies have suggested that temperature sensitivities of efflux components are highest in appropriately moist conditions and are suppressed under dry and excessively moist conditions (Wang et al., 2006; Jassal et al., 2008; Craine and Gelderman, 2011). Therefore, in the range of dry to adequately moist condition, an increase in soil moisture is likely to have increased the annual Q_{10} of efflux components. In our study site, soil moisture at the depth of 10 cm was significantly higher in post-thinning years, likely due to a decrease in canopy transpiration.

Annual R_s and R_h were lower than the values estimated based on the relationship between MATs and annual F_c in pre-thinning years, and those values were out of the 95% prediction intervals (Fig. 4a, b). Low precipitation in 2016 and suppressed litter decomposition are possible reasons for the lower values of annual R_s and R_h than expected. Total precipitation in the growing season in 2016 (788 mm) was the lowest among 12 years of measurement (1213 ± 298 mm, average ± 1SD during growing season for 12 years). Decreased precipitation was expected to cause a dry environment in the organic surface layer or litter layer (O horizon). Previous studies have demonstrated that litter decomposition is positively related with precipitation (Austin and Vitousek, 2000; Salamanca et al., 2003). Thus, low precipitation likely

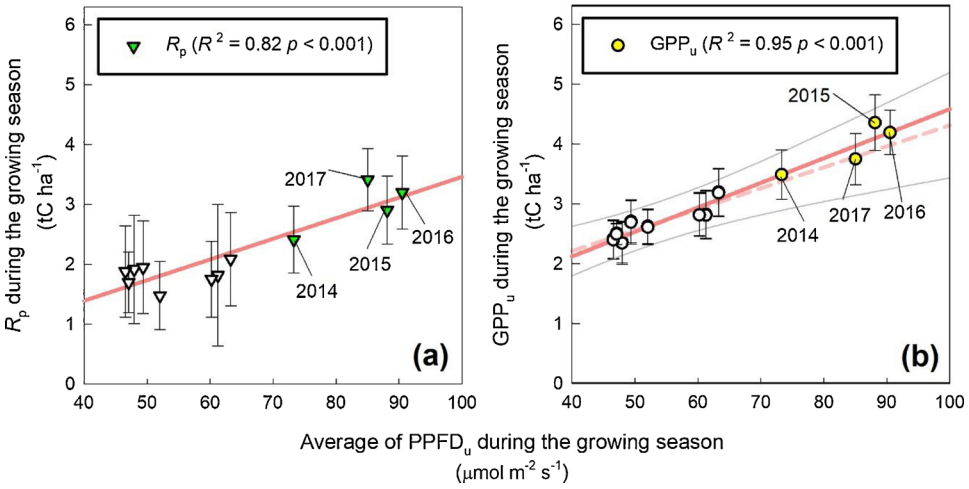

Fig. 7. Relationships between the averaged understory PPFD (PPFD$_u$) and seasonal sum of (a) plant respiration (R_p) and (b) understory gross primary production (GPP$_u$) during the growing season from May to October. Empty symbols represent data in pre-thinning years and filled symbols represent data in post-thinning years. Dashed lines represent significant ($p < 0.01$) relationships between PPFD$_u$ and each flux component in pre-thinning years as shown in Teramoto et al. (2017), and a coloured solid line represents a significant relationship, including all the data for 12 years of measurement. The pair of grey curves show a 95% prediction interval based on the regression analysis in pre-thinning years. Values are mean ± SE.

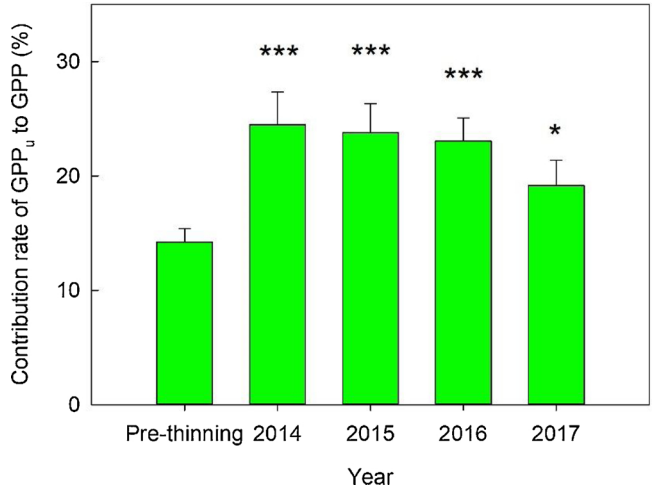

Fig. 8. Contribution rate of GPP_u to GPP. Asterisks shown as *, **, and *** represent the significant difference of that parameter compared to pre-thinning years at $p < 0.10$, $p < 0.05$, and $p < 0.01$, respectively. Values are mean ± SE.

suppresses litter decomposition that is a large (around 19–35%) component of R_s (Tan et al., 2013; Han et al., 2015; Sun et al., 2017a). Therefore, the lower R_s and R_h in 2016 are mainly attributed to the low precipitation and suppressed litter decomposition.

4.2. Impact of thinning on soil respiration (R_s) and soil heterotrophic respiration (R_h)

Previous studies show that thinning generally increases R_s due to increased temperature, improved resource partitioning to the remaining tree roots, root regrowth, and dead root decomposition (Zhang et al., 2018). In contrast, some studies report a decrease in R_s after thinning. Jonsson and Sigurdsson (2010) showed a decrease in R_s after 50–80% thinning in a young black cottonwood plantation in southern Iceland. The decrease in R_s after thinning can be explained by the decrease in living root density and root respiration (Tang et al., 2005). Overall, the influence of thinning on R_s is the result of complex interactions between the changes in environmental factors (e.g., soil temperature and soil moisture) and biotic factors (e.g., R_r and dead root decomposition).

In our study, annual R_s was significantly increased in 2015 (17.6%) compared to that in pre-thinning years. The significant increase can be mainly explained by the increased MATs. MATs in 2015 in soil chambers was 9.67 °C, which is 0.61 °C higher than the average value in pre-thinning years (2006–2013). Teramoto et al. (2017) reported that the annual R_s increased by 25.1% per 1 °C increase in MATs in the pre-thinning years in this larch forest. Thus, we can estimate a 15.2% increase in the annual R_s in 2015 compared to the pre-thinning years, caused by an increase in MATs by 0.61 °C (Fig. 4a).

The contribution ratio of R_h to R_s (R_h:R_s) theoretically increases after thinning, as thinning decreases R_r. This has been shown for *Pinus massoniana* stands in China by Lei et al. (2018). However, in our study, we did not observe such an increase in the R_h:R_s in the post-thinning years (75.8%, average for three years) compared with that in pre-thinning years (81.5%). The reason for this might be due to the decreased amount of larch leaf litterfall in post-thinning years. A meta-analysis by Zhang et al. (2018) based on 404 observations showed that thinning decreased litterfall by 23.7%. In our study site, the amount of larch leaf litterfall in pre-thinning years was 2.03 ± 0.31 t ha^{-1} (Table 1). After the first thinning, larch leaf litter fall decreased to 1.30 t ha^{-1} (−36.0%) in 2014 (the smallest litterfall among 2006–2017), gradually recovered (1.72 t ha^{-1} (−15.3%) in 2015, the second smallest litterfall among 2006–2017) to the pre-thinning level in 2016 (2.05 t ha^{-1}, Table 1).

4.3. Impact of thinning on understory light environment and total understory respiration (R_u)

The observed increase in $PPFD_u$ was the most apparent change in the understory environmental conditions caused by thinning. In our study, 39% thinning resulted in a 63.1% increase in $PPFD_u$. Our results are consistent with a previous study conducted in central Korea, which showed that 40% thinning in a larch plantation increased $PPFD_u$ by 59.4% (Son et al., 2004).

During the post-thinning years, annual R_u was significantly increased by 26.9% (Table 2). The increase in R_{15} of R_u in post-thinning years suggests that the increase in R_u is mostly independent of the change in soil temperature (Table 3). By focusing on the changing rate of flux components in R_u (R_p and R_s) in post-thinning years (average for three years), a significant increase was detected in R_p but not in R_s (Table 2). Therefore, the increase in R_u can mainly be attributed to the increase in R_p. The average increased ratio of R_p was 99.7% in post-thinning years as compared to that in pre-thinning years (Table 2). The increase in R_p is strongly related to the increase in understory plant biomass. Understory herbaceous plant biomass ranged from 220.1 to 364.3 g m^{-2} in 2017 at our study site. Upon comparison of this result with the understory herbaceous plant biomass data from August to September in pre-thinning years as reported by Arase (2012), the increase in understory herbaceous plant biomass was estimated to be 35.1% ($p = 0.047$). The increase of understory plant biomass in post-thinning years is consistent with a previous study by Son et al. (2004), reporting that thinning primarily increased $PPFD_u$ and resulted in increases in understory species richness and biomass. In addition, the summed growing season R_p was positively related to the average growing season $PPFD_u$ (Fig. 7a). These points indicate that the increase in $PPFD_u$ was the main driver of the increase in R_p via the increase in understory plant biomass. Although we observed some significant relationships between annual R_p and MATs (Fig. 4d) or average soil moisture (Fig. 6d), the contributions of these environmental factors to the increase of R_p in post-thinning years were minor if compared with the impact of increased $PPFD_u$.

4.4. Impact of thinning on understory photosynthesis (GPP_u)

Thinning significantly increased the GPP_u in post-thinning years (59.5% on average, Table 2). In a study estimating the understory productivity in a boreal forest in Finland, Kolari et al. (2006) implied the possible increase of understory productivity under improved light environment because the understory is generally light-limited. In fact, Teramoto et al. (2017) showed that the average growing season $PPFD_u$ changed dramatically due to canopy disturbance by a typhoon and a short summer drought. As a result, the annual GPP_u increased linearly along with the increase in the growing season $PPFD_u$ in their study. Our result is consistent with that reported by Cheng et al. (2017), who showed that thinning enhanced the net photosynthetic rate of understory herbaceous plants in a subtropical Masson's pine plantation in southern China. Increased GPP_u will accelerate carbon allocation within the understory plant structure and increase the understory biomass.

In this study, increased GPP_u in post-thinning years as compared to that in pre-thinning years (Table 2) played an important role to offset the decrease in canopy GPP. Vesala et al. (2005) reported that increased understory photosynthesis after thinning could partially compensate for the decrease in canopy photosynthesis in a boreal forest in Finland. In an oak plantation in England, Wilkinson et al. (2016) did not observe a change in carbon balance after thinning, and the authors suggest that increased photosynthesis of understory vegetation and the shrub layer compensated for the decrease in canopy photosynthesis. However, long-term and continuous measurements of understory photosynthesis to evaluate the effect of thinning on understory productivity are

inadequate. Litterfall and canopy GPP measurements at our study site also indicate that the ecosystem carbon gain of a Japanese larch plantation can recover within four years after thinning (Takahashi et al., *unpublished data*). As compared to the period from 2014 to 2016, the apparent decrease of the GPP_u:GPP ratio in 2017 implies a coupled effect between the recovery of canopy GPP (increase) and LAI and the resulting decrease of $PPFD_u$ and GPP_u in 2017 (Fig. 8).

4.5. Impact of tree thinning on net understory CO_2 exchange (NUE)

Annual NUE was higher in 2015. By focusing on the change of efflux components in NUE, R_p and R_s were significantly higher in 2015 than in pre-thinning years. As described above, the increased $PPFD_u$ was the main driver for the increase of R_p in post-thinning years. In the case of R_s, high MATs in 2015 likely caused this increase. The combined increase of these efflux components contributed to the significant increase of NUE in 2015. Changes of NUE in post-thinning years in 2016 and 2017 were not significant because the increased R_u was largely offset by increased GPP_u (Table 2).

Some previous studies using eddy-covariance measurements reported that light (21%) or moderate (25–43%) thinning did not significantly affect the ecosystem carbon balance (Saunders et al., 2012; Wilkinson et al., 2016). These studies imply the robustness of the total carbon balance in forest ecosystems after an artificial disturbance such as thinning. In our study, continuous observation using multi-channel large automated chambers demonstrate that understory flux components R_p, R_u, and GPP_u increased strongly in post-thinning years, but NUE was relatively robust compared with these enhanced understory flux components. However, a marginally significant increase of NUE in post-thinning years (the average of NUE from 2015 to 2017) implied a slight increase in NUE after 39% thinning in this larch forest.

4.6. Uncertainty caused by the chamber effect and trench treatment

The automated chamber method is used as a powerful tool for measuring the understory carbon flux (McGinn et al., 1998; Liang et al., 2003; Gaumont-Guay et al., 2009). However, chamber deployment inevitably influences the environmental parameters inside chambers like temperature, input of litterfall, precipitation, and $PPFD_u$. For example, air temperature inside the chamber increases along with the length of the measurement period in case the chamber consists of clear materials like plexiglass (Matthias et al., 1980). Rochette and Hutchinson (2005) suggested a significant increase in air and soil temperature during long measurement period (> 1 h). The measurement period in our study was 5 min, and chambers were kept open except for the measurement period. The short measurement period contributes to minimize the increase in temperature during measurement. In addition, the chamber size in our study (90 cm in length × 90 cm in width × 50 cm in height for soil chambers, 90 cm in length × 90 cm in width × 100 cm in height for plant chambers) is the largest among those used in previous studies (Liang et al., 2017). Combined with the short measurement period, large chamber size contributes to reduce the difference in precipitation and the amount of litter fall (leaves and small branches can be kept inside chambers) inside and outside the chambers. Further, we diminished the modification of $PPFD_u$ in the chambers using transparent PVC walls (transmittivity of PPFD through these PVC materials was about 70 to 80% as is written in materials and methods). Therefore, although uncertainty caused from chamber effects are inevitable when using the chamber method, we minimized the influence of these artefacts on understory carbon flux measurement as possible by using a large transparent automated chamber system with a short measurement period.

We used trench treatment to quantitatively evaluate R_h, but this method also causes uncertainty due to disturbance around chambers. We need to take the potential influence of trench treatment into consideration for evaluating R_h. First, trench treatment increases soil moisture due to reduced water uptake by roots (Epron et al., 1999). In our study, soil moisture was the highest in trenched plots during the growing season in post-thinning years (2015–2017). Second, trench treatment restricts root litter supplement. Root litter decomposition is an important component of R_h (Bowden et al., 1993), and restriction of root litter supplement might be a cause for underestimation of R_h (Epron, 2010). However, trench treatment is the most convenient and commonly used method for measuring R_h in the field, and the influence of artefacts arising from trench treatment on the evaluation of R_h is still under debate (Epron, 2010). At least in our study, trench treatment was an appropriate method because it enables us to exclude roots with smallest disturbance compared with other methods like artificial gap treatment (Nakane et al., 1996) or girdling treatment (Högberg et al., 2001).

5. Conclusion

Thinning (39%) altered the understory microclimate and increased the $PPFD_u$, soil temperature, and soil moisture in a larch plantation in central Japan. Increased $PPFD_u$ enhanced GPP_u and resulted in increased understory vegetation biomass, which consequentially increased both the R_p and R_u. On the other hand, increased GPP_u offset the increase in R_u in post-thinning years. Increased GPP_u also partly compensated the decreased canopy GPP in post-thinning years and contributed to the rapid recovery of ecosystem GPP after thinning. As a result, a significant increase in NUE was detected in 2015, but not in 2016 and 2017. This point suggests the relative robustness of the understory carbon balance after thinning compared with the largely enhanced understory flux components (R_p, R_u, and GPP_u). However, a marginally significant increase of NUE in post-thinning years (the average of NUE from 2015 to 2017) implied a slight increase in NUE after 39% thinning in this larch forest.

Declaration of interest

The authors declare no conflicts of interest for this manuscript.

Acknowledgements

We greatly thank Dr. Carolina Voigt of Université de Montréal for valuable comments on this manuscript. We also greatly appreciate Dr. Tetsuo Okano and Dr. Hajime Kobayashi of Shinshu University for providing biomass data. In addition, we thank Mr. Hidenori Tanabe of Fusokogyo Co., Ltd., and Dr. Hajime Tomimatsu, Mr. Yukio Yamao, and Mr. Yasuo Hirose of National Institute for Environmental Studies (NIES) for field maintenance, Dr. Akio Takenaka of NIES for the identification of understory plant species. This work was supported by the Environment Research and Technology Development Fund (2-1705) of the Environmental Restoration and Conservation Agency and by the Global Environment Research Account for National Institutes (Evaluation of the potential effect of global warming on soil carbon emission of Japanese forest ecosystems) of the Ministry of the Environment, Government of Japan. This study was also partially supported by the National Institute for Environmental Studies (NIES) Internal Call for Research Proposals (A) of 2014 (Evaluation of soil CO_2 efflux of Asian forest ecosystems based on an automated chamber network), by the Climate Change Adaptation Research Program of NIES, by the Global Environmental Monitoring Program and the Climate Change Research Program of the NIES, and by Grants-in-Aid for Scientific Research (grant number 16K00573) from the Japanese Ministry of Education, Culture, Sports, Science and Technology.

References

Arase, T., 2012. Estimation of seasonal changes of the biomass of forest floor vegetation in a larch forest at the northern foot of Mt. Fuji, Japan. J. Environ. Inform. Sci. 40,

23–30.
Austin, A.T., Vitousek, P.M., 2000. Precipitation, decomposition and litter decomposability of metrosideros polymorpha in native forests on Hawai'i. J. Ecol. 88, 129–138.
Bergeron, O., Margolis, H.A., Coursolle, C., 2009. Forest floor carbon exchange of a boreal black spruce forest in eastern North America. Biogeosciences 6, 1849–1864.
Binkley, D., Stape, J.L., Ryan, M.G., 2004. Thinking about efficiency of resource use in forests. For. Ecol. Manage. 193, 5–16.
Bowden, R.D., Nadelhoffer, K.J., Boone, R.D., Melillo, J.M., Garrison, J.B., 1993. Contributions of aboveground litter, belowground litter, and root respiration to total soil respiration in a temperature mixed hardwood forest. Can. J. For. Res. 23, 1402–1407.
Cheng, C., et al., 2017. Thinning effect on understory community and photosynthetic characteristics in a subtropical pinus massoniana plantation. Can. J. For. Res. 47, 1104–1115.
Craine, J.M., Gelderman, T.M., 2011. Soil moisture controls on temperature sensitivity of soil organic carbon decomposition for a mesic grassland. Soil Biol. Biochem. 43, 455–457.
Dore, S., et al., 2012. Recovery of ponderosa pine ecosystem carbon and water fluxes from thinning and stand-replacing fire. Global Change Biol. 18, 3171–3185.
Epron, E., 2010. Separating autotrophic and heterotrophic components of soil respiration: lessons learned from trenching and related root exclusion experiments. In: Kutsch, W.L., Bahn, M., Heinemeyer, A. (Eds.), Soil Carbon Dynamics: An Integrated Methodology. Cambridge University Press, Cambridge, pp. 157–168.
Epron, D., Farque, L., Lucot, E., Badot, P.M., 1999. Soil CO_2 efflux in a beech forest: the contribution of root respiration. Ann. Forest Sci. 56, 289–295.
FAO, 2015. Global Forest Resources Assessment 2015: How Are the World's Forests Changing? UN Food and Agriculture Organization, Rome.
Forest Agency, 2012. Japan Forest Resources Assessment. 2012. Ministry of Agriculture, Forestry and Fisheries, Japan. http://www.rinya.maff.go.jp/j/keikaku/genkyou/h24/index.html.
Gaumont-Guay, D., et al., 2009. Soil CO_2 efflux in contrasting boreal deciduous and coniferous stands and its contribution to the ecosystem carbon balance. Global Change Biol. 15, 1302–1319.
Grassi, G., et al., 2017. The key role of forests in meeting climate targets requires science for credible mitigation. Nat. Clim. Change 7, 220–228.
Han, T.F., Huang, W.J., Liu, J.X., Zhou, G.Y., Xiao, Y., 2015. Different soil respiration responses to litter manipulation in three subtropical successional forests. Sci. Rep. 5, 18166.
Harper, C.W., Blair, J.M., Fay, P.A., Knapp, A.K., Carlisle, J.D., 2005. Increased rainfall variability and reduced rainfall amount decreases soil CO_2 flux in a grassland ecosystem. Global Change Biol. 11, 322–334.
Högberg, P., et al., 2001. Large-scale forest girdling shows that current photosynthesis drives soil respiration. Nature 411, 789–792.
Jassal, R.S., Black, T.A., Novak, M.D., Gaumont-Guay, D., Nesic, Z., 2008. Effect of soil water stress on soil respiration and its temperature sensitivity in an 18-year-old temperate douglas-fir stand. Global Change Biol. 14, 1305–1318.
Jonsson, J.A., Sigurdsson, B.D., 2010. Effects of early thinning and fertilization on soil temperature and soil respiration in a poplar plantation. Iceland. Agr. Sci. 23, 97–109.
Kolari, P., et al., 2006. Forest floor vegetation plays an important role in photosynthetic production of boreal forests. For. Ecol. Manage. 221, 241–248.
Lei, L., et al., 2018. Thinning but not understory removal increased heterotrophic respiration and total soil respiration in *Pinus massoniana* stands. Sci.Total. Environ. 621, 1360–1369.
Liang, N., Inoue, G., Fujinuma, Y., 2003. A multichannel automated chamber system for continuous measurement of forest soil CO_2 efflux. Tree Physiol. 23, 825–832.
Liang, N., Hirano, T., Zheng, Z.M., Tang, J., Fujinuma, Y., 2010. Soil CO_2 efflux of a larch forest in northern Japan. Biogeosciences 7, 3447–3457.
Liang, N., Teramoto, M., Takagi, M., Zeng, J., 2017. High-resolution data on the impact of warming on soil CO_2 efflux from an Asian monsoon forest. Sci. Data 4, 170026.
Liu, X.Z., Wan, S.Q., Su, B., Hui, D.F., Luo, Y.Q., 2002. Response of soil CO_2 efflux to water manipulation in a tallgrass prairie ecosystem. Plant Soil 240, 213–223.
Lloyd, J., Taylor, J.A., 1994. On the temperature-dependence of soil respiration. Funct. Ecol. 8, 315–323.
Matthias, A.D., Blackmer, A.M., Bremner, J.M., 1980. A simple chamber technique for field measurement of emissions of nitrous oxide from soils. J. Environ. Qual. 9, 251–256.
McGinn, S.M., Akinremi, O.O., McLean, H.D.J., Ellert, B., 1998. An automated chamber system for measuring soil respiration. Can. J. Soil Sci. 78, 573–579.
Morris, D.M., Hills, S.C., Bowling, C., 1994. Growth and form responses to pre-commercial thinning regimes in aerially seeded jack pine stands: 5th year results. Forest. Chron. 70, 780–787.
Nakane, K., Kohno, T., Horikoshi, T., 1996. Root respiration rate before and just after clear-felling in a mature, deciduous, broad-leaved forest. Ecol. Res. 11, 111–119.
Pan, Y.D., et al., 2011. A large and persistent carbon sink in the world's forests. Science 333, 988–993.
Peltola, H., Miina, J., Rouvinen, I., Kellomaki, S., 2002. Effect of early thinning on the diameter growth distribution along the stem of Scots pine. Silva Fenn. 36, 813–825.
Rochette, P., Hutchinson, G.L., 2005. Measurement of soil respiration in situ: chamber techniques. In: In: Hatfield, J.L., Baker, J.M. (Eds.), Micrometeorology in Agricultural Systems ASA-CSSA-SSSA. Agron. Monogr. 47. pp. 247–286.
Ruiz-Peinado, R., Bravo-Oviedo, A., Lopez-Senespleda, E., Bravo, F., del Rio, M., 2017. Forest management and carbon sequestration in the mediterranean region: a review. Forest Syst. 26, eR04S.
Salamanca, E.F., Kaneko, N., Katagiri, S., 2003. Rainfall manipulation effects on litter decomposition and the microbial biomass of the forest floor. Appl. Soil Ecol. 22, 271–281.
Saunders, M., et al., 2012. Thinning effects on the net ecosystem carbon exchange of a sitka spruce forest are temperature-dependent. Agr. Forest Meteorol. 157, 1–10.
Son, Y., Lee, Y.Y., Jun, Y.C., Kim, Z.-S., 2004. Light availability and understory vegetation four years after thinning in a *Larix leptolepis* plantation of central Korea. J. For. Res-Jpn. 9, 133–139.
Sun, L.F., Teramoto, M., Liang, N., Yazaki, T., Hirano, T., 2017a. Comparison of litter-bag and chamber methods for measuring CO_2 emissions from leaf litter decomposition in a temperate forest. J. Agric. Meteorol. 73, 59–67.
Sun, X., et al., 2017b. Change in evapotranspiration partitioning after thinning in a Japanese cypress plantation. Trees 31, 1411–1421.
Sundqvist, E., Vestin, P., Crill, P., Persson, T., Lindroth, A., 2014. Short-term effects of thinning, clear-cutting and stump harvesting on methane exchange in a boreal forest. Biogeosciences 11, 6095–6105.
Swanson, R.V., Flanagan, L.B., 2001. Environmental regulation of carbon dioxide exchange at the forest floor in a boreal black spruce ecosystem. Agric. Forest Meteorol. 108, 165–181.
Takahashi, Y., et al., 2015. Characteristics of temporal variations in ecosystem CO_2 exchange in a temperate deciduous needle-leaf forest in the foothills of a high mountain. J. Agric. Meteorol. 71, 302–317.
Tan, Z.-H., et al., 2013. Soil respiration in an old-growth subtropical forest: patterns, components and controls. J. Geophys. Res. Atmos. 118, 2981–2990.
Tang, J., Qi, Y., Xu, M., Misson, L., Goldstein, A.H., 2005. Forest thinning and soil respiration in a ponderosa pine plantation in the Sierra Nevada. Tree Physiol. 25, 57–66.
Teramoto, M., Liang, N.S., Takagi, M., Zeng, J.Y., Grace, J., 2016. Sustained acceleration of soil carbon decomposition observed in a 6-year warming experiment in a warm-temperate forest in southern Japan. Sci. Rep. 6, 35563.
Teramoto, M., Liang, N., Zeng, J., Saigusa, N., Takahashi, Y., 2017. Long-term chamber measurements reveal strong impacts of soil temperature on seasonal and inter-annual variation in understory CO_2 fluxes in a Japanese larch (*Larix kaempferi* sarg.) forest. Agric. Forest. Meteorol. 247, 194–206.
Teramoto, M., Liang, N.S., Ishida, S., Zeng, J.Y., 2018. Long-term stimulatory warming effect on soil heterotrophic respiration in a cool-temperate broad-leaved deciduous forest in northern Japan. J. Geophys. Res. Biogeosci. 123, 1161–1177.
Vesala, T., et al., 2005. Effect of thinning on surface fluxes in a boreal forest. Global Biogeochem. Cycles 19, GB2001.
Wang, C.K., Yang, J.Y., Zhang, Q.Z., 2006. Soil respiration in six temperate forests in China. Global Change Biol. 12, 2103–2114.
Wilkinson, M., Crow, P., Eaton, E.L., Morison, J.I.L., 2016. Effects of management thinning on CO_2 exchange by a plantation oak woodland in south-eastern England. Biogeosciences 13, 2367–2378.
Yuste, J.C., Nagy, M., Janssens, I.A., Carrara, A., Ceulemans, R., 2005. Soil respiration in a mixed temperate forest and its contribution to total ecosystem respiration. Tree Physiol. 25, 609–619.
Zeng, J., Nojiri, Y., Landschutzer, P., Telszewski, M., Nakaoka, S., 2014. A global surface ocean fCO_2 climatology based on a feed-forward neural network. J. Atmos. Ocean. Technol. 31, 1838–1849.
Zhang, X., et al., 2018. The effects of forest thinning on soil carbon stocks and dynamics: a meta-analysis. For. Ecol. Manage. 429, 36–43.
Zhou, L., et al., 2016. Thinning increases understory diversity and biomass, and improves soil properties without decreasing growth of Chinese fir in southern China. Environ. Sci. Pollut. Res. 23, 24135–24150.